

Extended atmosphere of the yellow hypergiant V509 Cas in 1996–2018

V.G. Klochkova, E.L. Chentsov, V.E. Panchuk

Special Astrophysical Observatory RAS, Nizhnij Arkhyz, 369167 Russia

January 25, 2019

Abstract Based on the data of spectral monitoring of the yellow hypergiant V509 Cas performed in 1996–2018 at the 6-m telescope with the spectral resolution of $R \geq 60\,000$, we studied in detail its kinematic state at various levels of extended atmosphere. No signs of presence of a companion were found. An agreement of radial velocities measured on the permitted and forbidden emissions of metal ions, as well as their strict temporal stability led us to the choice of the systemic velocity of the star $V_{\text{sys}} = -63$ km/s. The position of forbidden [NII] emissions forming in the circumstellar medium is strictly stable and is systematically shifted by -6 km/s relative to the metal ion emissions. A conclusion on the variation of the [NII] emission halfwidths and intensities (the lines have become narrower and more intense) is made after the observations in 1996 and these parameters did not vary over the next 22 years of observations. The velocities measured from the shortwave FeII(42) absorption components are located in a narrow interval of $V_r = -(84 \div 87)$ km/s, which indicates the stability of expansion of the upper layers of the atmosphere. The overall atmosphere of the hypergiant is stable, excluding the layers close to the photosphere. The velocity variability in range of $V_r = -(52 \div 71)$ km/s, identified by the positions of strong metal ion absorption cores, may be a manifestation of pulsations in deep atmospheric layers, where this type of lines are formed.

Key words. stars: massive–stars: evolution–stars: atmospheres: individual: V509 Cas

1. Introduction

A yellow hypergiant V509 Cas is a prominent representative of a group of rare stars near the luminosity limit. The general data about these objects with the initial masses of $20 \div 40 M_{\odot}$ are represented in [1, 2]. In addition to their extreme luminosity, yellow hypergiants differ from ordinary supergiants by a very high mass-loss rate in the stellar wind and the presence of gas and dust circumstellar envelope. Hypergiant instability is manifested as a weak brightness variability (with an amplitude of $\approx 0.2 \div 0.4^m$), which is usually referred to as the pulsation type. Along with the manifestations of instability, yellow hypergiants also experience sporadic pulsations, the so-called “shell episodes”, during which the star is particularly intensively losing its mass and for several hundreds of days gets enveloped by the ejected cold matter forming a pseudophotosphere.

Yellow hypergiants occupy a limited area on the Hertzsprung–Russell diagram [3]. However, observable properties of well-studied representatives of this family (ρ Cas, V509 Cas, V1302 Aql) significantly differ. This has to do primarily with the differences in the optical spectra and the features of the structure and kinematics of the envelopes. For example, in the spectrum of the yellow hypergiant ρ Cas, which is considered as a prototype of a group of yellow hypergiants, a significant variability of the emission-absorption profile $H\alpha$, as well as the splitting of the BaII, SrII, TiII and other strongest absorptions with a low excitation potential of the lower level was discovered more than half a century ago by Bidelman and McKellar [4]. Later, these features of the ρ Cas spectrum were studied in detail

by spectral monitoring [5–9]. On the HR diagram ρ Cas is located at the boundary of the Yellow Void [2], separating the hypergiants and LBVs in the quiet phase. On the boundary of the Yellow Void, the amplitude of pulsations of yellow hypergiants apparently sharply increases, what leads to an increased instability of the atmosphere and a blowing off of the envelope [2]. In 2013, the ρ Cas system underwent a new mass ejection, at which the stars brightness dropped by 0.5^m . This ejection occurred only 12 years after the previous one in 2000–2001. This way, there is an increase in ejections in ρ Cas, which, according to Aret et al. [10] may suggest an approach of the star to the boundary of the Yellow Void. Surprisingly, with such a vigorous mass loss, an optical spectrum so rich in features and variability, this hypergiant does not have a circumstellar dust envelope.

A close relative of ρ Cas, a yellow hypergiant V1302 Aql, is on the contrary associated with one of the brightest sources of IR-radiation IRC+10420. In the system of this object a source of maser radiation in OH was also detected [11]. The optical spectrum of V1302 Aql is dominated by the emission and absorption lines of metal ions FeII, TiII, ScII, CrII, emission lines FeI and absorption lines NI, OI and SiII, as well as the forbidden lines [FeII], [CaII] and [OI] [12–15]. Metal ion line profiles are very diverse: from almost symmetrical emissions to the reverse P Cyg-type profiles and absorption profiles with two emission components. A long-term spectral monitoring of V1302 Aql, performed during the past decades [12, 14, 15], led to the conclusion that the object had passed on the HR-diagram the path from the red supergiant to the cold border of the Yellow Void.

The difficulty of studying the spectra of yellow hypergiants is well-illustrated by the history of the study of the cool supergiant HD 179821, identified with an IR source IRAS 19114+0002. A combination of the observed parameters of this star for a long time did not allow to unambiguously determine its evolutionary status (see the paper [16] and references therein). However, over the past years, strong enough evidence for the belonging of the star to yellow hypergiants was obtained [17, 18]. The supergiant V509 Cas, like V1302 Aql, described a complex path, a “zigzag” on the HR-diagram, as expressed in [3]. In the optical wavelength range the spectrum of this hypergiant varied at different points of observation in the range of spectral classes G–K, while preserving the Ia luminosity class [19]. The optical spectrum of V509 Cas is rich in emission features that distort the absorption profiles not only of hydrogen, but also of metallic lines, which in one way or another is inherent in the spectra of other studied yellow hypergiants. At the same time, the spectrum of V509 Cas revealed a unique feature—emissions of highly excited forbidden lines of [NII] 6548 and 6584 Å already found in the spectrum of this star in 1961 [20], when this star was considered as an MK-classification standard. Their presence in the spectrum of such a cool single star is difficult to explain. This fact served as an incentive for us to conduct a long-term monitoring of the star with high spectral resolution.

In this paper, we present the results obtained based on the monitoring of the spectrum of the star over several sets in 1996–2018. Section 2 briefly describes the methods of observations and data analysis. In Section 3 we present the results, compare them with the ones previously published. Section 4 gives the conclusions.

2. Observations, reduction and analysis of spectra

We have carried out all observations of V509 Cas with the echelle spectrographs in the Nasmyth focus of the 6-m BTA telescope of the Special Astrophysical Observatory of the RAS. The dates of observations and registered spectral ranges are given in Table 1. In 1996 we used the Lynx echelle spectrograph [21], which in combination with the CCD chip 1K×1K provided the spectral resolution of $R \approx 25\,000$. All subsequent spectral data were obtained with the NES echelle spectrograph [22, 23], equipped with a large format CCD sized 2048×4608 pixels. To reduce light loss without a deterioration of spectral resolution, the NES spectrograph is equipped with an image slicer (which provides three slices of a stellar image). Every spectral order on the image is repeated three times with an offset along the dispersion of an echelle grating [23]. A transition to the large format CCD substantially extended the boundaries of the simultaneously recorded wavelength interval: for example, $\Delta\lambda = 5400 \div 8479$ Å in the

Table 1. Heliocentric radial velocity V_r measurements, rounded to the nearest km/s, in the spectra of V509 Cas from sets of various types of lines

Date	$\Delta\lambda$, nm	Vr, km/s											
		[FeII] emis	lines of ions			FeII(42) abs	H α abs	[NII]	NaI				DIBs
			emis	wing	core				CS	st	IS	IS	
1	2	3	4	5	6	7	8	9	10	11	12	13	14
02.05.1996	527-685	-62	-62	-62	-71		-104, -11	-69	-89	-62	-47	-15	-14
03.07.1996	515-800	-63	-62	-63	-66		-103, -20	-68	-88	-62	-48	-14	-15
01.10.2014	540-848	-63	-63	-60	-53		-96, -18	-69	-90	-62	-50	-14	-13
04.09.2015	395-666	-62	-63	-62	-60	-87, -55	-96, -22	-69	-90	-62	-51	-14	-15
26.10.2015	398-676	-63	-63	-63	-62	-87, -53	-95, -22	-68	-90	-62	-50	-14	-14
12.02.2017	470-778	-62	-63	-62	-59	-84, -52	-93, -27	-69	-89	-62	-50	-13	-14
13.06.2017	470-778	-63	-63	-63	-62	-86, -54	-92, -26	-69	-89	-62	-50	-14	-14
03.08.2017	470-778	-63	-64	-63	-62	-85, -54	-92, -21	-69	-89	-62	-52	-14	-14
06.04.2018	470-778	-63	-62	-61	-59	-84, -55	-93, -20	-68	-89	-61	-52	-14	-14

spectrum of 1.10.2014 or $\Delta\lambda=4697\div7782$ Å in the spectra of 2017. Spectral resolution is $\lambda/\Delta\lambda \geq 60\,000$, the signal-to-noise ratio is $S/N > 100$ and differs little from one spectrum to another.

Extraction of one-dimensional data from the twodimensional echelle spectra was performed using an ECHELLE context from the MIDAS software package modified taking into account the features of the echelle frames of the spectrographs used (see the features in [24]). The removal of traces of cosmic particles was carried out by the median averaging of two spectra, obtained sequentially one after the other. The wavelength calibration was performed based on the spectra of a Th–Ar hollow-cathode lamp. We identified the features in the spectrum of V509 Cas using the previously published spectral atlas [25]. All further reduction, including the photometric and positional measurements was done using the latest version of the DECH20t code [26]. Note that this spectrum reduction program we traditionally use allows to measure radial velocities for individual features of line profiles, and that the paper only uses the heliocentric velocities V_r . Systematic errors in measuring V_r , estimated by sharp interstellar components of NaI do not exceed 0.25 km/s (from one line), a random error for shallow absorptions of about 0.7 km/s – the average value per line. Thereby for our averaged values in Table 1 random errors are about 0.3 km/s.

3. Discussion of results

3.1. Main features of the optical spectrum of V509 Cas

V509 Cas is a very attractive object for a detailed high-resolution spectroscopy: this bright star has coordinates, permitting year-round observations in the northern hemisphere, and its spectrum is abound in a variety of complex features, which can be clearly seen in Figs. 1–3. Naturally, such an interesting object has a long history of spectral observations, and the main features of its spectrum were found in the earliest publications [20]. Since 1974, its spectral class has become earlier: in 1977 it was classified as F8 (the same as in ρ Cas [19]). According to our observations, from 1996 to 2018 the spectrum of V509 Cas varied little, and the spectral class remained even earlier, close to F2. We made this estimate visually from a comparison of the spectrum of V509 Cas with the data from the spectral atlas of F- and G-stars [25] and quantitatively from the FeI and FeII line intensity ratio. Figure 4 shows the evolution of the stellar spectrum with time on its small fragment with the FeI and FeII lines. Two upper fragments are borrowed from the above work [19]. This figure indicates the absence of significant changes of spectral class in V509 Cas during our observations over 1996–2018, which is consistent with the constancy of the effective temperature of the star during these years (see Fig. 2 in [3]).

As noted in the Introduction, in terms of its effective temperature and its evolutionary status V509 Cas is close to a related object V1302 Aql. The optical spectrum of the hypergiant V1302 Aql is

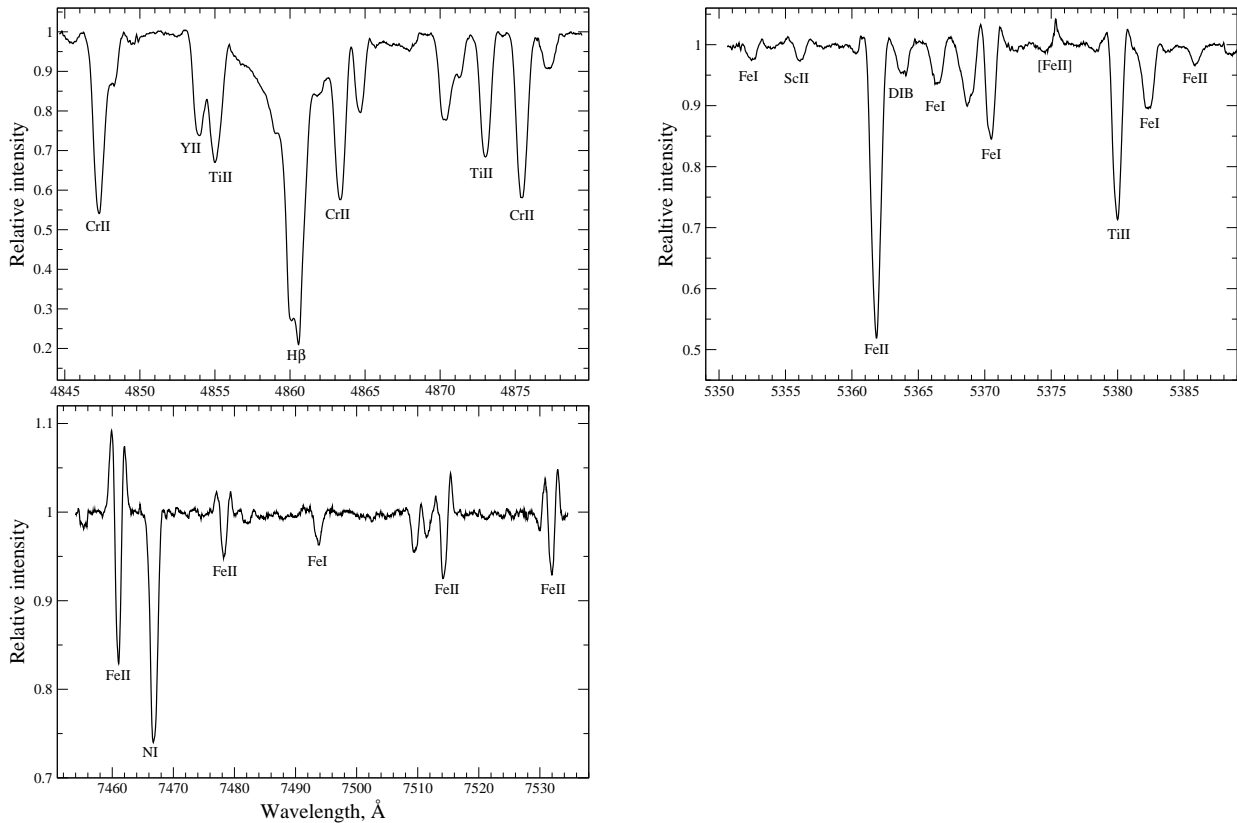


Figure 1. Fragments of the spectrum of V509 Cas: (a) the interval of $4845\div 4880\text{ \AA}$, containing the $H\beta$ line; (b) the interval of $5350\div 5390\text{ \AA}$ with the forbidden line $[\text{FeII}]\ 5376\text{ \AA}$; (c) the interval of $7455\div 7535\text{ \AA}$ with the $\text{NI}\ 7468\text{ \AA}$ line. The main features are identified.

dominated by the emission and absorption lines of FeII , TiII , ScII , CrII metal ions, FeI emission lines and NI , OI and SiII absorptions [14, 27]. Some emission features are identified with the forbidden lines of $[\text{FeII}]$, $[\text{CaII}]$ and $[\text{OI}]$. The metal ion line profiles are very diverse: from the almost symmetrical emissions to the reverse P Cyg-like profiles and absorption profiles with two emission components. The high excitation lines (NI , OI and SiII) have almost symmetrical absorption profiles, shifted on the average by 5 km/s red-wave relative to the positions of minima of their profiles. The spectra of V509 Cas reveal roughly the same set of metal lines, but the FeI lines are more often purely absorption, or absorption with emissions in the wings.

The hydrogen $H\alpha$ and $H\beta$ lines in the spectra of V1302 Aql have a characteristic two-peak profile, similar to the $H\alpha$ profile in the spectrum of V509 Cas. But compared to the spectrum of V509 Cas, the ratio of emission peaks in the spectrum of V1302 Aql is the opposite: the short-wave peak is much more intense than the long-wave peak. Only on one of the dates (11/24/2007) of many years of monitoring of V1302 Aql the 6-m telescope recorded an unusual view of the $H\alpha$ profile, in which the longwave peak substantially exceeds the shortwave one. In addition, unlike V509 Cas, in the spectrum of V1302 Aql a broad photospheric absorption is completely flooded with the emission. For a more detailed comparison of the spectra of two hypergiants it is convenient to use the atlas of the V1302 Aql spectrum [28].

All our spectra of V509 Cas contain the $H\alpha$ line, some of its profiles are presented in Fig. 3, from which stems an insignificant profile variability over the whole period of 1996–2018. The intensity of the shortwave emission peak is constantly below the longwave one. Mainly the shortwave absorption wing is exposed to the wind-induced variability. There are no noticeably significant changes either in the shapes of metal line profiles or in the positions of their main components. This is shown in

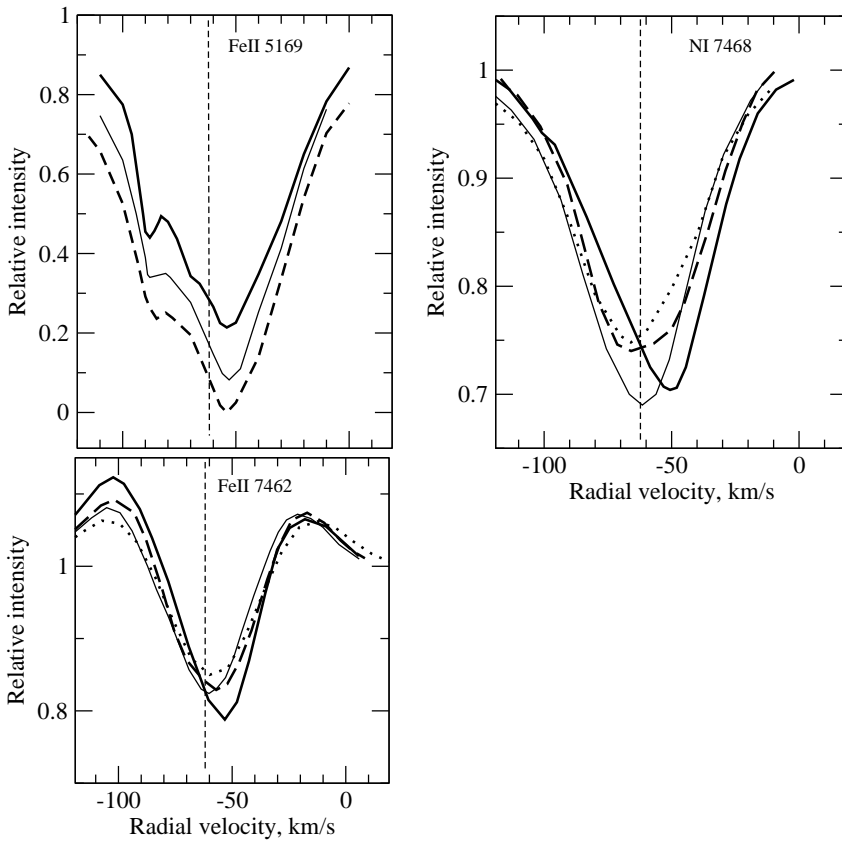


Figure 2. The variations of line profiles in the spectra of V509 Cas obtained over different years: the dotted line – in 1996, the solid thick line — in 2014, the solid thin line – in 2017, the dashed line – in 2018. The FeII 5169 Å line profiles are shifted along the ordinate axis with respect to the previous profile by 0.1. The vertical dashed line indicates the accepted value of systemic velocity $V_{\text{sys}} = -63$ km/s.

Fig. 2, which demonstrates the absorption profiles of NI 7468 and FeII 5169 AA (fragments with the profile of FeII 5169 Å are shifted vertically relative to the top one) the absorption-emission profile of the FeII 7462 Å line, as well as Table 1.

V509 Cas is usually considered to be a spectral twin of the hypergiant ρ Cas [29], and therefore many authors compare their spectra [5, 29–31]. However, a detailed study of the spectra of both hypergiants with close fundamental parameters (mass, luminosity, evolutionary stage) revealed significant differences both in the spectra and kinematic conditions of their atmospheres, indicating differences in physical processes causing an instability of the atmospheres and envelopes. Spectral differences are manifested primarily in the differences of the $H\alpha$ profile and its variability.

The $H\alpha$ profile in the spectrum of ρ Cas significantly varies mainly due to the envelope ejections. The $H\alpha$ profile variations are especially demonstrative after the 2013 ejection [9]. The shifts of the $H\alpha$ profile indicate a change in structure and increased instability of the upper layers of the extended atmosphere of the star. A significant shift of the profile to the long-wavelength region in the spectra of August–September 2017 indicates the infall of the layers of matter where the line is formed.

As follows from Fig. 3, the behavior of $H\alpha$ profile in the spectrum of V509 Cas is according to our observations more calm. The $H\alpha$ absorption components in this figure and FeII (42) lines in Fig. 2 are located on both sides of the V_{sys} line, which indicates the presence in the atmosphere and in the envelope of V509 Cas of both the outflowing and accreting matter. The profile variations are observed in the shift and variable width of the absorption component (Fig. 3) caused by unstable conditions in

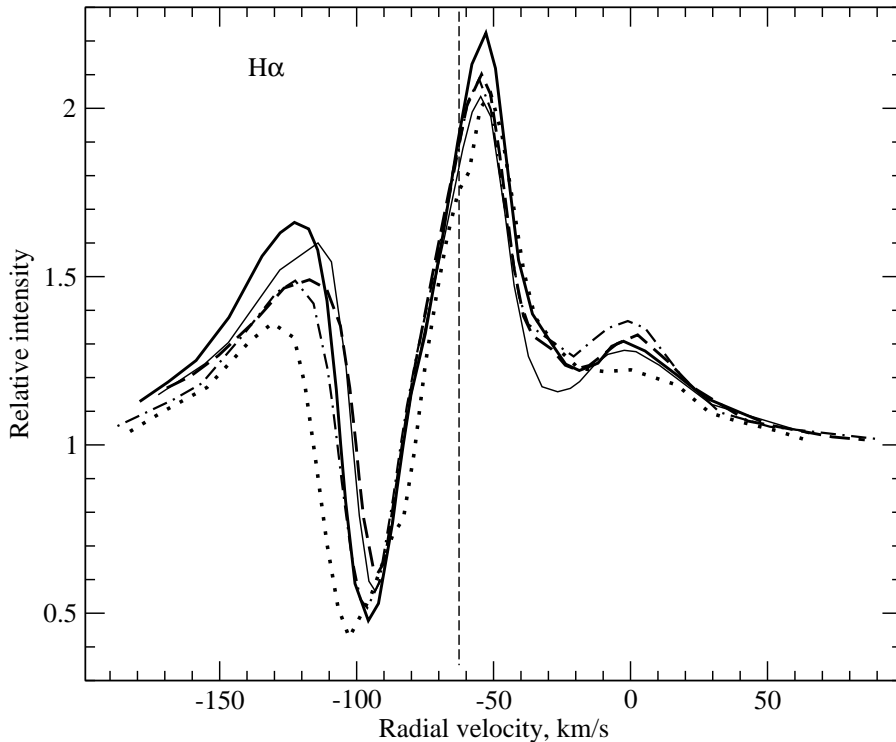


Figure 3. The variations of the $H\alpha$ profile in the spectra of V509 Cas obtained on various dates: 05/02/1996 – the dotted line, 10/01/2014 – the thick solid line, 10/26/2015 – the dash-dotted line, 2017 – the thin solid line, 04/06/2018 – the dashed line. Vertical dashed line indicates the accepted value of the systemic velocity $V_{\text{sys}} = -63$ km/s.

the envelope, expanding at a velocity of $33\div 40$ km/s. Note that the authors of [30], comparing the spectra of V509 Cas and ρ Cas in the near UV, have also emphasized that these two stars are not spectral twins.

In addition, a temporarily variable splitting of the strongest absorptions and envelope emissions of the iron group atoms is observed in the spectrum of ρ Cas (see [9] and the references therein). Both of these effects due to the presence of a powerful structured envelope in ρ Cas, are absent in the spectrum of V509 Cas. On the other hand, the spectrum of V509 Cas possesses the features missing in the spectrum of ρ Cas: the highly excited forbidden lines [NII] and emission components in most of the permitted and forbidden metal ion lines (see article [20] and Fig. 1 and 4 in this publication). A number of diffuse interstellar features are identified in the spectrum of V509 Cas, while they are absent in the spectrum of ρ Cas, which has close galactic coordinates.

The spectrum of V509 Cas has a similarity with the spectrum of a hotter high-luminosity star 3 Pup (Sp = A4 Iabe). In the spectrum of this massive supergiant, studied in detail in [32], a bifurcated $H\alpha$ line was registered with a stronger red component (a P Cyg III-type profile according to Beals [33]), the emissions of forbidden [OI] 1F 6300, 6364 Å lines, the doublet [CaII] 1F 7291, 7324 Å and emissions in some Fe II lines. The authors of [32] stressed that in the spectrum of 3 Pup only the MgII 4481 Å line can be considered photospheric, and in FeII lines a contribution of the envelope is obvious, which gives the profiles a specific shape: the wings are raised by the emissions. The same type of features we also observe in the spectrum of V509 Cas, in which the wings of even the weak lines are distorted by the emissions, which is clearly seen in Fig. 2 for the FeII 7462 Å line with a depth of not more than 0.2 from the level of the local continuum. The star 3 Pup is the coldest member of the family of supergiants with the B[e] phenomenon, discussed in detail in the paper of Aret et al. [34].

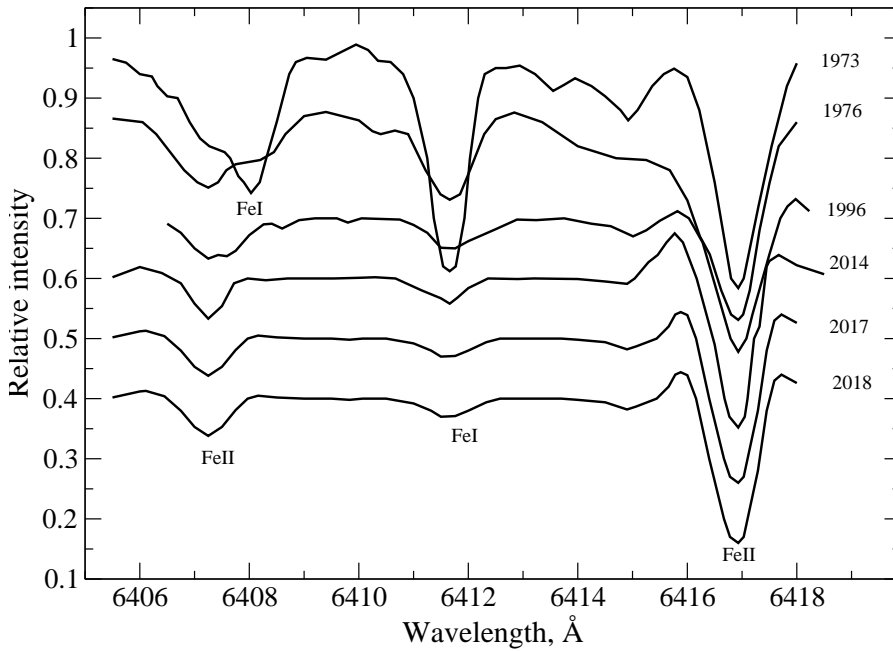


Figure 4. Variability of the spectrum of V509 Cas in the wavelength range of 6405–6418 Å. The two upper curves are adopted from [19].

Table 2. The results of measurements of the parameters of [NII] lines in the spectra of V509 Cas. Half-widths of δV_r profiles are rounded to whole km/s, the equivalent widths W_λ are given in Å. Uncertain values are marked by the colon.

Date	[NII] 5755		[NII] 6548		[NII] 6583	
	δV_r	W_λ	δV_r	W_λ	δV_r	W_λ
1961 ¹					50	
1967 ²				0.045	30	0.13
2.05.1996	20	0.025	30	0.10	29	0.33
3.07.1996	19	0.026	32	0.17:	28	0.33
1.10.2014	13	0.045	21	0.13	23	0.43
4.09.2015	14	0.047	21	0.12	24	0.42
26.10.2015	15	0.048	23	0.13	24	0.45
12.02.2017	13	0.041	24	0.14	24	0.46
13.06.2017	15	0.047	20	0.14	23	0.44
3.08.2017	14	0.041	19	0.14	22	0.41
6.04.2018	14	0.041	22	0.14	23	0.46

1 – the data from [20], 2 – the data from [44].

3.2. Forbidden lines of [NII]

The presence of various emission combinations [OI], [OII], [NII], [SII], [CaII], etc. is not a sign of any certain class of stars. Strong forbidden emissions whose region of formation is a dense rotating disk [34] are ordinary features in the spectra of stars with the B[e] phenomenon. An example of this class of stars are the well known star CI Cam and above-mentioned 3 Pup, in the spectrum of which there are many forbidden emissions, but the [NII] emissions are absent. The presence of forbidden emissions is known in other types of hot, far evolved stars that have passed stages with a substantial loss of matter: a hypergiant MWC 314 [28], an LBV-star GR-290 [35], an X-ray transient [36, 37], a protoplanetary nebulae that entered the envelope ionization phase [38–42]. The objects with forbidden emissions of light metals and their ions are often binary systems with a hot component [43].

It is also well known that the optical spectra of classical symbiotic and symbiotic nova stars as a rule contain forbidden emissions. An example could be a cool peculiar supergiant PU Vul [45, 46]. Symbiotic stars are binary systems with a hot companion, UV radiation of which provides ionization of the gas envelope of the system and formation of the emission spectrum [47]. However, for the spectrum of a single cold star V509 Cas the presence of [NII] emissions are more difficult to explain. The likely mechanisms of excitation of these emissions in the spectrum of V509 Cas are discussed in many publications since the discovery of these features. Sargent [20] notes that the presence of forbidden [NII] emissions and complex emission-absorption $H\alpha$ and $H\beta$ profiles indicate the probable existence around V509 Cas of a hot envelope. In the article [48], devoted to the study of the chemical composition of the atmosphere of V509 Cas, Luck adheres to the same position. However, Lambert et al. [5] do not find this version with a hot companion attractive, calling it only a passive spectator of the cataclysms of the primary star. As long ago as in 1978 Lambert and Luck [19] suggested several versions on the mechanism of excitation of forbidden [NII] lines in the spectrum of V509 Cas: dissipation of mechanical energy, ionization due to the UV radiation of hot stars of an HII-region in the volume of the Cep OB1 association etc. Obviously, the principal in solving this problem is the spectrum of V509 Cas in the UV range. As the authors of [30] showed, the UV spectrum of this star does not contain any features and fully meets the expectations given the main parameters of this object.

A peculiar behavior of [NII] emissions is observed in the spectrum of the cold peculiar supergiant R CrB. In a state of a deep brightness minimum, when the star is almost completely closed, optimal conditions arise for the registration of a nebular spectrum of the envelope [49]. An important moment is a long duration of the glare of the envelope in the [NII] emissions: as noted by the authors of [50], at low density, the nebula can remain ionized for up to 10^4 years.

In the spectrum of V509 Cas, the half-width of the [NII] lines varies: $\delta V_r = 50$ km/s in September 1961 [20], 30 km/s in 1967 [44]. The half widths for three lines [NII] 5755, 6548 and 6583 Å are measured from our spectra, presented in Table 2. It is necessary to emphasize here that the half widths measured in our spectra by five times exceed the half-width of the spectrographs point spread function. A reduction of the emission half-widths in the spectra of V509 Cas occurred after the 1996 observations and persisted over the next 22 years of our observations. The intensities of the [NII] lines also vary with time: in 1967 the equivalent widths W_λ of the 6583 and 6548 Å lines were 0.13 and 0.045 Å respectively [44], which is consistent with the theoretical intensity ratio 3:1 according to Osterbrock [51]. According to our observations the behavior of line half-widths with time was accompanied by a synchronous change in their intensities: in 1996 the equivalent widths increased by approximately 1.7 times, then the intensity stabilized. Note that in the spectrum of the star the intensity measurements were carried out relative to the level of the local continuous spectrum, so that at the constant emission rate in lines, their variability is also possible due to the varying brightness of a star. According to the AAVSO database, V509 Cas experiences a slight brightness decrease in the past decade. Since the half-width also varies, it means that the velocity dispersion changes in an optically thin envelope, i.e. the envelope is non-stationary.

3.3. Radial velocity pattern

We have fully identified the features in the spectrum of V509 Cas. However, their huge number does not allow us to give here a complete list of identified lines. Table 3 contains only those spectral features, the positions of which are measured to study the velocity field. Expecting to find a probable velocity field stratification in the extended atmosphere of the hypergiant, we conducted a subsequent analysis of radial velocity measurements, by combining the related spectral features into several groups. Group averages are presented in Table 1, where the dates of spectrum acquisition are indicated (in 1996 using the Lynx spectrograph, further – using the NES spectrograph), the working spectral intervals and heliocentric radial velocities V_r , averaged for the spectral features of different nature and rounded to whole km/s.

The third column of Table 1 lists the averaged velocities for the forbidden [FeII] emissions (10–13 features in the spectra with different wavelength ranges), while the fourth column gives them for the permitted metal ion emissions. The subsequent columns for the features of other types:

- such as the paired elevations above the continuous spectrum on the absorption wings (see the FeII 7462 Å profile in Fig. 2) (over two hundred absorptions of SiII, ScII, TiII, CrII, FeII, YII, BaII). The listed values are given for the emissions in general, the central parts of which are superimposed by absorptions. The measurements are made from the lower parts of their profiles;
- for the upper parts of the profiles (wings) (fifth column) and FeI weak absorption cores (10–12 lines), CaI (four lines) – the sixth column;
- for the cores of the components of the three strong FeII absorptions of the 42-nd multiplet in column (7) (as an example, Fig. 2 shows the line profile of this multiplet FeII 5169 Å);
- for the absorption components (in column (8)) of the H α profile presented in Fig. 3;
- for three forbidden [NII] emissions 5755, 6548 and 6584 Å in column (9);
- for the four components of the NaI (1) profiles in columns (10)–(13). Figure 5 presents the NaI 5896 Å profile, averaged over the 2017 spectra;
- for a sample of diffuse interstellar DIB bands with the wavelengths λ : 5705, 5780, 5797, 5849, 6196, the last 6203, 6284, 6379, 6613, 6660, 6672 Å – in the last column.

Owing to the high quality of the spectra and a long-term monitoring, we have obtained reliable conclusions in our study regarding the temporal behavior of the velocity field in the atmosphere of V509 Cas, which follow from the data in Table 1. The proximity of the values presented in the first three columns, and their constancy in time indicate that the systemic velocity of V509 Cas is close to $V_{\text{sys}} = -63$ km/s. Exactly this value is described by a vertical broken line in Figs. 2 and 3. Note that the accepted value of the systemic velocity $V_{\text{sys}} = -63$ km/s is not so far from the average velocity for the Cep OB1 association $V_r = -58.2$ km/s [52], a member of which is also the hypergiant V509 Cas. Variations of velocity measured from the forbidden lines (3-d column of Table 1) are minimal over time: $V_r = -(62 \div 63)$ km/s. The velocity variability for the cores of FeII (42) absorptions is also minimal: $V_r = -(84 \div 87)$ km/s, what testifies to the stability of the upper atmosphere. Note a similar behavior in time of the positions of forbidden emissions and FeII (42) core absorptions in the spectrum of the above-mentioned supergiant 3 Pup [32].

As follows from Table 1 (column 6), velocity variability is the most prominent by the positions of strong absorption cores of the iron group ions: their range from these absorptions is $V_r = -(52 \div 71)$ km/s. This variability, which is well-illustrated by a panel with an NI 7468 profile in Fig. 2, in the case of a single star can be a manifestation of pulsations in the deep atmospheric layers, where the formation of this type of lines takes place. A pulsation variability of radial velocity in highly excited lines of neutral nitrogen NI with a full amplitude of about 19 km/s coinciding with our result was previously found by Sheffer and Lambert [29]. They found probable variability periods of 421 and 315 days, noting a constant, incessant profile instability. Recall that this type of pulsation variability with an amplitude of about 10 km/s measured from the weak and moderate-intensity symmetric absorptions is also inherent in the hypergiant ρ Cas [9].

As follows from the data of Table 1, forbidden [NII] emissions in the spectrum of V509 Cas are systematically shifted relative to the [FeII] emissions. However, this shift is stable, since for all times of our observations, the position of the [NII] emission remains in a small interval of velocities: $V_r(\text{NII}f) = -(68 \div 69)$ km/s. A temporal constancy of this velocity is noted by Lambert et al. [5], taking the mean value of $V_r(\text{NII}f) = -72$ km/s for systemic velocity. Additional justification for this choice of systemic velocity follows from the agreement of $V_r(\text{NII}f)$ with a velocity measured from the emissions

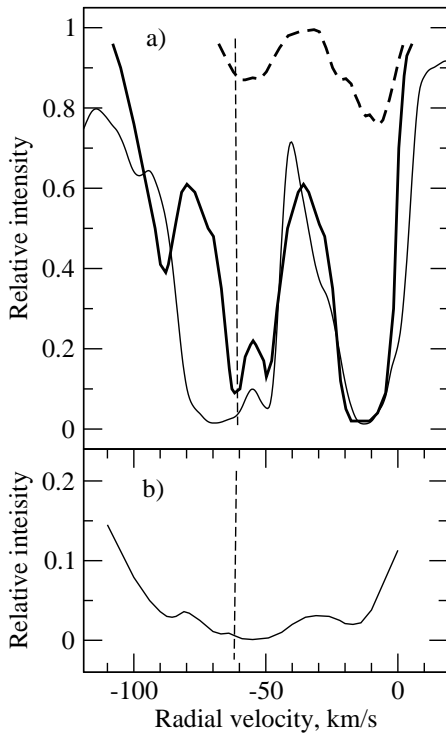


Figure 5. The profiles of selected features: (a) NaI 5896 D-lines in the spectrum of V509 Cas are represented by the solid line, and in the spectrum ρ Cas – by the thin line. The dashed line marks the profile of KI 7699 Å in the spectrum of V509 Cas; (b) the CaII 3968 Å line in the spectrum of V509 Cas. The vertical dashed line describes the accepted value of systemic velocity $V_{\text{sys}} = -63$ km/s for V509 Cas.

of a CO molecule, forming at the most outer layers of the extended atmosphere of the hypergiant: $V_r(\text{CO}) = -(72 \div 76)$ km/s [5]. Later, the conclusion about the constancy of the radial velocity measured from the forbidden emissions of [NII] in the optical spectra obtained during the long-term monitoring was also done by Sheffer and Lambert: $V_r(\text{NII}f) = -72$ km/s [29] and $V_r(\text{NII}f) = -69$ km/s [53].

A remnant of ejection of stellar matter located at a distance from the star can be considered a possible source of radiation of forbidden [NII] emissions. Earlier, de Jager [54] proposed such an explanation for the occurrence of forbidden [NII] emissions in spectrum of V509 Cas, indicating the formation of these emissions in the envelope, the kinetic temperature in which is higher than the temperature of the star. One has to keep in mind that the atmosphere of the star, and hence the matter ejected in the circumstellar neighborhood are largely enriched with nitrogen, because in the atmosphere of V509 Cas the nitrogen excess is over $+3.5$ dex [48]. Apparently, the so much altered chemical composition of the atmosphere explains the lack of expected emissions of oxygen ions, the relative abundance of which in the atmosphere of the star is at least two orders of magnitude lower than that of nitrogen [48].

3.4. Multicomponent profile of NaI D-lines

Multicomponent profiles of NaI D-lines (see Table 1 and Fig. 5a), in addition to the component near the systemic velocity, also contain a narrow absorption with $V_r \approx -50$ km/s and the poorly resolved in our spectra saturated components in the velocity range of $V_r \approx -20; -30$ km/s. A narrow absorption of $V_r \approx -50$ km/s is formed in the interstellar medium and corresponds to the position of V509 Cas farther away than the Perseus Arm [55, 56]. The positions of the circumstellar components in Fig. 5, where the NaI D-line profiles in the spectra of V509 Cas and ρ Cas are compared [9], having close

galactic coordinates, are in a good agreement. An interstellar feature of $V_r = -13$ km/s is registered in the spectrum of the variable V354 Lac [57], the galactic coordinates of which are close to those for V509 Cas and ρ Cas.

The structure of interstellar lines in the spectrum of V509 Cas agrees well with its great remoteness, as well as with its extremely high luminosity, $M_V \approx -9^m$. We obtained the luminosity estimate based on the equivalent width $W_\lambda(\text{OI } 7774) = 2.35 \text{ \AA}$ of the triplet OI 7774 \AA in the spectrum of the star using the calibrations from [14, 58]. For comparison note that in the spectrum of the hypergiant V1302 Aql with its extreme luminosity near the Humphreys–Davidson limit [59, 60], the equivalent width of the oxygen triplet has a maximum value of $W_\lambda(\text{OI } 7774) = 2.8 \text{ \AA}$ [14].

The position of the NaI component with the velocity $V_r = -62; -63$ km/s in Fig. 5 is close to the emissions and absorption wings, which indicates the formation of this component in the stellar atmosphere. The position of the most shortwave depression in the NaI D line profiles coincides with the shortwave component of the FeII (42) profiles: -89 km/s in Fig. 2. This agreement indicates the formation of the most shortwave component in the outermost layers of the atmosphere close to the circumstellar envelope. A broad long-wave component of the NaI D-lines in the velocity range of $V_r \approx -20; -30$ km/s includes several unresolvable (at $R = 60\,000$) interstellar features. The position of one of them coincides with the reliably measured in the spectrum of V509 Cas position of diffuse interstellar bands (DIBs): of about -14 km/s.

The KI 7699 \AA profile features, also presented in Fig. 5, mostly correspond to those of the NaI D-lines. However, interstellar bands of $V_r \approx -14$ and -23 km/s, formed in the Local Arm are better identified in this profile. All these features of the interstellar and circumstellar origin are discernible in the core of the CaII 3968 \AA line in Fig. 5b.

4. Conclusions

Based on the data of spectral monitoring of the yellow hypergiant V509 Cas, performed over 1996–2018 at the 6-m telescope with spectral resolution $R \geq 60\,000$, its kinematic state at various levels of extended atmosphere was studied in detail. The proximity of velocities based on the permitted and forbidden emissions of metal ions, as well as their strict constancy in time led to the choice of systemic velocity of the hypergiant: $V_{\text{sys}} = -63$ km/s.

No signs of binarity of the star were detected.

For all our observations sets, the position of forbidden [NII] emissions, forming in the circumstellar medium, corresponds to the velocity $V_r(\text{NII f}) = -(68 \div 69)$ km/s. Therefore, [NII] emissions are systematically shifted by -6 km/s relative to the metal ion emissions. We made a conclusion that after the 1996 the variation of half widths and [NII] emission intensities (the lines have become narrower and more intense) and over the next 22 years of observations, these parameters did not vary.

The velocities determined using the cores of wind absorptions FeII (42) are constant within the interval of $V_r = -(84 \div 87)$ km/s, which indicates the stability of the uppermost layers of the atmosphere.

In general, we concluded on the stability of the hypergiants atmosphere excluding the layers closest to the photosphere. The velocity variability in range of $V_r = -(52 \div 71)$ km/s, determined by the positions of the cores of strong absorptions of the metal group ions may be a manifestation of pulsations in the deep atmospheric layers, where this type of lines is formed.

Acknowledgements. VGK thanks the Russian Science Foundation for the partial financial support (project 14-50-00043). ELCh and VEP thank the Russian Foundation for Basic Research for the partial support (projects nos. 16-02-00587a and 18-02-00029a). This work made use of the SIMBAD, SAO/NASA ADS, AAVSO and VALD astronomical databases.

References

1. R. M. Humphreys, *Astrophys. J. Suppl.* **38** 309 (1978).
2. C. de Jager, *Astron. Astrophys. Rev.* **8** 145 (1998).
3. H. Nieuwenhuijzen, C. De Jager, I. Kolka, et al., *Astron. and Astrophys.* **546** A105 (2012).
4. W. P. Bidelman and A. McKellar, *Publ. Astron. Soc. Pacif* **69** 31 (1957).
5. D. L. Lambert, K. H. Hinkle, and D. N. B. Hall, *Astrophys. J.* **248** 638 (1981).
6. A. Lobel, G. Israelian, C. de Jager, et al., *Astron. and Astrophys.* **330** 659 (1998).
7. N. Gorlova, A. Lobel, A. J. Burgasser, et al., *Astrophys. J.* **651** 1130 (2006).
8. V. G. Klochkova, V. E. Panchuk, and N. S. Tavalzhanskaya, and I. A. Usenko, *Astron. Reports* **58** 101 (2014).
9. V. G. Klochkova, V. E. Panchuk, and N. S. Tavalzhanskaya, *Astron. Reports* **62** 623 (2018).
10. A. Aret, M. Kraus, I. Kolka, G. Maravelias. In: “The B[e] Phenomenon: Forty Years of Studies”. *Proceed. of a Conf. held at Charles University, Prague, Czech Republic 27.06–01.07.2016*. Eds. by A. Miroshnichenko, S. Zharikov, D. Korčáková and M. Wolf. San Francisco: ASP Conf. Ser, **508** 357 (2017).
11. P. T. Giguere, N. J. Woolf, and J. C. Webber, *Astrophys. J.* **207** L195, (1976).
12. V.G. Klochkova, E.L. Chentsov, and V. E. Panchuk, *Monthly Notices Royal Astron. Soc.* **292** 19 (1997).
13. R. D. Oudmaijer, *Astron. and Astrophys. Suppl.* **129** 541, (1998)
14. V. G. Klochkova, M. V. Yushkin, E. L. Chentsov, and V. E. Panchuk, *Astron. Reports* **46** 139 (2002).
15. V. G. Klochkova, E. L. Chentsov, A. S. Miroshnichenko, et al., *Monthly Notices Royal Astron. Soc.* **459** 4183 (2016).
16. B. E. Reddy and B. J. Hrivnak, *Astron. J.* **117** 1834 (1999).
17. R.D. Oudmaijer, B. Davies, W.-J. de Wit, and M. Pa tel, *ASP Conf. Ser.* **412** 17 (2009).
18. T. Sahin, D. L. Lambert, V. G. Klochkova, and V. E. Panchuk, *Monthly Notices Royal Astron. Soc.* **461** 4071 (2016).
19. D. L. Lambert and R. E. Luck, *Monthly Notices Royal Astron. Soc.* **184** 405 (1978).
20. W. L. W. Sargent, *Observatory* **85** 33 (1965).
21. V. E. Panchuk, V. G. Klochkova, G. A. Galazutdinov, et al., *Astron. Letters* **19** 431 (1993).
22. V. E. Panchuk, V. G. Klochkova, M. V. Yushkin, and I. D. Najdenov, *Preprint No.179, SAO RAS (Spec. Astrophys. Obs., Nizhnij Arkhyz, 2003)*.
23. V. E. Panchuk, V. G. Klochkova, and M. V. Yushkin, *Astron. Reports* **61** 820 (2017).
24. M. V. Yushkin and V. G. Klochkova, *Preprint No. 206, SAO RAS (Spec. Astrophys. Obs., Nizhnij Arkhyz, 2005)*.
25. V. G. Klochkova, S. V. Ermakov, and V. E. Panchuk, *Preprint No. 157, SAO RAS (Spec. Astrophys. Obs., Nizhnij Arkhyz, 2001)*.
26. G. A. Galazutdinov, *Preprint No.92, SAO RAS (Spec. Astrophys. Obs., Nizhnij Arkhyz, 1992)*.
27. R. M. Humphreys, K. Davidson, and N. Smith, *Astron. J.* **124** 1026 (2002).
28. E. L. Chentsov, V. G. Klochkova, and N. S. Tavalganskaya, *Bull. Spec. Astrophys. Obs.* **48** 25 (1999).
29. Y. Sheffer and D. L. Lambert, *Publ. Astron. Soc. Pacif* **99** 1277 (1987).
30. G. Israelian, A. Lobel, and M. R. Schmidt, *Astrophys. J.* **523** L145 (1999).
31. R. B. Stothers, *Astrophys. J.* **751** 151 (2012).
32. E. L. Chentsov, V. G. Klochkova, and A. S. Miroshnichenko, *Astrophys. Bulletin* **65** 150 (2010).
33. C. S. Beals, *Publ. Dominion Astrophys. Obs. Victoria*, **9** 1 (1953).

34. A. Aret, M. Kraus, and M. Slechta, *Monthly Notices Royal Astron. Soc.* **456** 1424 (2016).
35. V. F. Polcaro, C. Rossi, R. F. Viotti, et al., *Astron. J.* **141** 18 (2011).
36. A. S. Miroshnichenko, V. G. Klochkova, K. S. Bjorkman, and V. E. Panchuk, *Astron. and Astrophys.* **390** 627 (2002).
37. E. A. Barsukova, N. V. Borisov, A. N. Burenkov, et al., *Astron. Reports* **50** 664 (2006).
38. M. Parthasarathy, G. Gauba, T. Fujii, Y. Nakada, In: Szczerba R., Górny S.K. (eds). *Post-AGB Objects as a Phase of Stellar Evolution. Astrophys. & Space Sci. Library, Springer, Dordrecht*, **265**, 29 (2001).
39. V. P. Arkhipova, N. P. Ikonnikova, R. I. Noskova, et al., *Astron. Letters* **27** 719 (2001).
40. V. P. Arkhipova, V. G. Klochkova, E. L. Chentsov, et al., *Astron. Letters* **32** 661 (2006).
41. G. Sarkar, D.A. Garca-Hernandez, M. Parthasarathy, et al., *Monthly Notices Royal Astron. Soc.* **421** 679 (2012).
42. V. G. Klochkova, E. L. Chentsov, V. E. Panchuk, et al., *Astrophys. Bulletin* **69** 439 (2014).
43. A. Lobel, C. Martayan, A. Mehner, J.H. Groh, In: “The B[e] Phenomenon: Forty Years of Studies”. *Proceed. of a Conf. held at Charles University, Prague, Czech Republic 27.06–01.07.2016*. Eds. by A. Miroshnichenko, S. Zharikov, D. Korčáková and M. Wolf. San Francisco: ASP Conf. Ser, **508**, 245 (2017).
44. G. H. Herbig, *Contr. Lick Obs.* **276** (1969).
45. T. S. Belyakina, N. I. Bondar, D. Chochol, et al., *Astron. and Astrophys.* **223** 119 (1989).
46. M. Kato, J. Mikoajewska, and I. Hachisu, *Astrophys. J.* **750** 5 (2012).
47. R.L.M. Corradi, J. Mikolajewska, T.J. Mahoney, In: “Symbiotic Stars Probing Stellar Evolution”, *ASP Conf Proceed*, Edited by R.L.M. Corradi, J. Mikolajewska and T.J. Mahoney. San Francisco: ASP Conf Ser, **303**, (2003).
48. R. E. Luck, *Astrophys. J.* **202** 743 (1975).
49. N. Kameswara Rao, D. L. Lambert, M. T. Adams, et al., *Monthly Notices Royal Astron. Soc.* **310** 717 (1999).
50. N. Kameswara Rao and D. L. Lambert, arXiv:1112.6225 (2011).
51. D. E. Osterbrock, *Astrophysics of Gaseous Nebulae and Active Galactic Nuclei*. University Science Books, Mill Valley, California. 408p. (1989).
52. A. M. Melnik and A. K. Dambis, *Monthly Notices Royal Astron. Soc.* **472** 3887 (2017).
53. Y. Sheffer and D. L. Lambert, *Publ. Astron. Soc. Pacif* **104** 1054 (1992).
54. C. de Jager, *The Brightest Stars* (D. Reidel Publ. CO, Dordrecht, 1980).
55. Y. P. Georgelin and Y. M. Georgelin, *Astron. and Astrophys.* **6** 349 (1970).
56. J. P. Vallee, *Astron. J.* **135** 1301 (2008).
57. V. G. Klochkova, *Astron. Letters* **35** 457 (2009).
58. A. Arellano Ferro, S. Giridhar, E. Rojo Arellano, *Revista Mexicana de Astronomía Astrofísica*, **39** 3 (2003).
59. R. M. Humphreys and K. Davidson, *Astrophys. J.* **232** 409 (1979).
60. T. J. Jones, R. M. Humphreys, R. D. Gehrz, et al., *Astrophys. J.* **411** 323 (1993).

Table 3: Residual intensities r and heliocentric radial velocities V_r (km/s) for individual lines in the high resolution spectrum of V509 Cas

Ident	λ	r	V_r
YII (6)	3950.35	0.74	-62
VII (10)	3951.96	0.66	-58
CaII (1)	3968.47	0.03	-86
		0.01	-55
		0.02	-17
H ϵ	3970.07	0.11	-59
TiII (11)	3981.99	0.61	-59
TiII (11)	3987.61	0.78	-59
FeII (126)	4012.46	0.33	-65
TiII (11)	4025.13	0.46	-62
TiII (87)	4028.34	0.43	-61
FeI (43)	4045.81	0.50	-60
CrII (19)	4051.97	0.75	-60
TiII (87)	5053.83	0.44	-58
FeI (43)	4063.59	0.59	-59
NiII (11)	4067.03	0.70	-60
FeI (43)	4071.74	0.66	-61
SrII (1)	4077.72	0.33	-61
H δ	4101.74	0.13	-58
CrII (18)	4110.99	0.75	-59
FeII (22)	4124.78	0.81	-57
ZrII (41)	4149.20	0.69	-61
TiII (21)	4161.52	0.60	-62
TiII (105)	4163.64	0.38	-59
TiII (105)	4171.90	0.44	-59
FeII (27)	4173.46	0.31	-58
FeII (28)	4178.85	0.31	-59
SrII (1)	4215.52	0.39	-60
FeII (27)	4233.17	0.20	-57
CrII, (31)	4242.37	0.58	-58
ScII (7)	4246.83	0.22	-59
FeII (28)	4258.15	0.62	-61
CrII (31)	4261.92	0.64	-59
FeII (32)	4278.15	0.78	-59
TiII (20)	4287.88	0.56	-60
TiII (41)	4290.21	0.27	-60
TiII (20)	4294.10	0.25	-61
FeII (28)	4296.57	0.50	-60
TiII (41)	4300.04	0.19	-58
TiII (41)	4307.89	0.30	-61
YII (5)	4309.63	0.82	-63
TiII (41)	4312.86	0.30	-58
TiII (20)	4337.92	0.25	-59
H γ	4340.47	0.14	-55
FeII (27)	4351.77	0.29	-58
TiII (104)	4367.66	0.63	-59
FeII (28)	4369.40	0.74	-59
FeII (27)	4385.38	0.42	-59
YII (5)	4398.02	0.82	-56
FeI (41)	4404.75	0.69	-60
TiII (51)	4407.68	0.87	-59
ScII (14)	4420.67	0.96	-61

Ident	λ	r	Vr
TiII (19)	4443.80	0.24	−59
TiII (19)	4450.48	0.41	−60
FeII (26)	4461.43	0.81	−61
TiII (40)	4464.45	0.56	−60
TiII (31)	4468.49	0.23	−58
TiII (40)	4470.85	0.68	−58
FeII (37)	4472.92	0.74	−58
MgII (4)	4481.22	0.44	−60
FeII (37)	4491.40	0.49	−60
TiII (31)	4501.27	0.25	−59
FeII (38)	4508.28	0.37	−59
FeII (37)	4515.34	0.41	−59
TiII (18)	4518.33	0.82	−58
FeII (37)	4520.22	0.41	−58
FeII (38)	4522.63	0.32	−58
TiII (82)	4529.49	0.67	−61
CrII (39)	4539.62	0.91	−58
FeII (38)	4541.52	0.56	−60
TiII (60)	4544.02	0.86	−61
TiII (30)	4545.14	0.83	−62
CrII (44)	4558.64	0.41	−59
TiII (50)	4563.76	0.26	−58
CrII (39)	4565.77	0.84	−61
TiII (82)	4571.97	0.21	−59
FeII (38)	4576.34	0.56	−60
FeII (38)	4583.83	0.27	−58
CrII (44)	4588.20	0.47	−60
CrII (44)	4592.05	0.69	−59
VII (56)	4600.19	0.93	−59
CrII (44)	4616.62	0.72	−59
CrII (44)	4618.82	0.55	−61
FeII (38)	4620.51	0.68	−60
FeII (37)	4629.33	0.38	−60
CrII (44)	4634.07	0.61	−59
FeII (37)	4666.75	0.67	−59
TiII (49)	4708.67	0.80	−61
FeII (43)	4731.47	0.61	−61
[FeII]20F	4774.72	1.03	−64
TiII (92)	4779.98	0.66	−60
TiII (17)	4798.53	0.86	−59
TiII (92)	4805.09	0.54	−60
CrII (30)	4812.35	0.84	−60
[FeII]20F	4814.53	1.05	−62
CrII (30)	4824.14	0.53	−60
CrII (30)	4836.24	0.83	−60
CrII (30)	4848.25	0.61	−61
H β	4861.33	0.21	−67
TiII (114)	4874.01	0.78	−62
CrII (30)	4876.40	0.65	−58
[FeII]4F	4889.62	1.09	−58
FeII (36)	4893.81	0.93	−59
[FeII]20F	4905.34	1.03	−61
TiII (114)	4911.19	0.71	−60
FeII (42)	4923.92	0.21	−56
BaII (1)	4934.08	0.80	−60
[FeII]20F	4947.37	1.02	−63

Ident	λ	r	Vr
[FeII]20F	4950.74	1.02	-61
FeII (36)	4993.35	0.81	-60
TiII (71)	5013.69	0.84	-62
FeII (42)	5018.44	0.49	-88
		0.22	-55
SiII (5)	5041.03	0.86	-62
SiII (5)	5056.06	0.83	-65
TiII (113)	5072.30	0.85	-60
YII (20)	5087.42	0.88	-63
ZrII (95)	5112.27	0.94	-59
FeII (35)	5120.34	0.94	-59
FeII	5123.19	0.95	-61
TiII (86)	5129.16	0.67	-61
FeII (35)	5132.67	0.92	-60
FeII (35)	5146.12	0.89	-62
TiII (70)	5154.08	0.68	-61
[FeII]	5158.78	1.06	-62
FeII (42)	5169.03	0.45	-88
		0.35	-70
		0.21	-54
MgI (2)	5172.69	0.68	-59
MgI (2)	5183.61	0.63	-60
TiII (86)	5185.91	0.70	-61
TiII (70)	5188.69	0.49	-61
FeII (49)	5197.58	0.48	-60
YII (20)	5200.41	0.92	-63
YII (20)	5205.73	0.86	-61
TiII (70)	5226.55	0.54	-60
FeII (49)	5234.62	0.45	-60
CrII (43)	5237.32	0.67	-60
ScII (26)	5239.82	0.84	-61
FeII	5254.93	0.79	-60
FeII (49)	5256.93	0.91	-59
FeII (48)	5264.80	0.74	-59
[FeII]18F	5273.35	1.10	-62
FeII (49)	5276.00	0.42	-58
FeII (41)	5284.10	0.66	-60
CrII (24)	5305.86	0.88	-59
CrII (43)	5308.42	0.90	-60
CrII (43)	5313.58	0.82	-59
FeII (48)	5316.66	0.36	-59
FeII (49)	5325.56	0.77	-59
FeI (15)	5328.04	0.88	-56
[FeII]19F	5333.65	1.04	-61
CrII (43)	5334.87	0.83	-58
ZrII (115)	5350.09	0.97	-61
FeII (48)	5362.87	0.57	-61
FeI (15)	5371.50	0.95	-61
[FeII]19F	5376.45	1.04	-61
TiII (69)	5381.03	0.80	-60
CrII (23)	5407.62	0.95	-60
TiII (69)	5418.78	0.85	-61
CrII (23)	5420.93	0.93	-64
FeII	5425.25	0.80	-61
FeI (15)	5429.70	0.96	-60
FeI (15)	5455.61	0.96	-58

Ident	λ	r	Vr
CrII (50)	5478.37	0.88	−63
TiII (68)	5490.69	0.96	−62
FeII (55)	5534.86	0.66	−60
[FeII]39F	5551.31	1.02	−61
FeI (686)	5615.64	0.94	−64
FeII (57)	5627.49	0.96	−59
ScII (29)	5640.98	0.90	−61
YII (38)	5662.95	0.88	−64
ScII (29)	5667.15	0.93	−62
ScII (29)	5669.03	0.90	−62
ScII (29)	5684.19	0.89	−63
NaI (6)	5688.21	0.95	−60
DIB	5705.20	0.96	−22
[NII]3F	5754.64	1.08	−67
DIB	5780.37	0.84	−20
FeII (164)	5823.15	0.99	−64
FeII (182)	5835.49	0.99	−62
DIB	5849.80	0.97	−16
BaII (2)	5853.68	0.97	−63
CaI (47)	5857.46	0.99	−62
NaI (1)	5889.95	0.21	−90
		0.09	−62
		0.16	−50
		0.02	−14
NaI (1)	5895.92	0.36	−90
		0.11	−62
		0.20	−51
		0.03	−14
SiII (4)	5978.93	0.93	−65
FeII (46)	5991.37	0.91	−60
FeII (46)	6084.10	0.94	−61
FeII (46)	6113.32	0.96	−63
CaI (3)	6122.22	0.97	−65
BaII (2)	6141.72	0.87	−63
FeII (74)	6147.74	0.80	−62
CaI (3)	6162.18	0.97	−64
DIB	6195.96	0.93	−14
FeII (162)	6199.19	0.99	−59
DIB	6203.08	0.94	−17
FeII (74)	6238.39	0.81	−60
ScII (28)	6245.62	0.92	−61
FeII (74)	6247.55	0.70	−59
DIB	6283.85	0.81	−22
SiII (2)	6347.10	0.60	−59
FeII (40)	6369.47	0.93	−60
SiII (2)	6371.36	0.67	−59
DIB	6379.29	0.94	−15
FeI (168)	6393.61	0.99	−65
FeI (816)	6400.01	0.99	−66
FeI (816)	6411.65	0.97	−57
FeII (74)	6416.93	0.84	−59
CaI (18)	6439.08	0.98	−65
FeII	6442.95	0.97	−65
FeII (74)	6456.38	0.60	−61
BaII (2)	6496.91	0.64	−56
[NII]1F	6548.03	1.12	−68

Ident	λ	r	Vr
H α	6562.81	0.52	−96
		1.27	−22
[NII]1F	6583.45	1.40	−70
DIB	6613.56	0.89	−16
DIB	6660.64	0.96	−11
DIB	6672.15	0.98	−10
TiII (112)	6717.91	0.93	−57
SI (8)	6748.79	0.97	−57
SI (8)	6757.16	0.96	−52
[FeII]14F	7155.14	1.08	−64
[CaII]1F	7291.46	1.24	
[FeII]14F	7388.16	1.03	−63
MnII (4)	7415.78	0.88	−52
FeII(73)	7462.39	0.80	−54
NI (3)	7468.31	0.70	−51
FeII (72)	7479.69	0.94	−53
FeII (73)	7515.79	0.91	−54
FeII (72)	7533.36	0.91	−54
KI (1)	7698.97	0.86	−61
		0.86	−56
		0.75	−11
FeII (73)	7711.71	0.76	−55
DIB	7721.85	0.96	−11
OI (1)	7771.94	0.40	−55
OI (1)	7774.17	0.41	
OI (1)	7775.39	0.48	−54
MgII (8)	7896.37	0.81	−55
H (P20)	8392.40	0.63	−58
H (P19)	8413.32	0.65	−57
H (P18)	8437.96	0.64	−55
OI (4)	8446.38	0.39	−52
H (P17)	8467.26	0.58	−53